International Journal of Innovative Computing, Information and Control
Volume **21**, Number **4**, August **2025**

ICIC International ©2025 ISSN 1349-4198
pp. 955–971

A NOVEL COMMAND-FILTERED BACKSTEPPING SLIDING MODE CONTROL OF THREE-PHASE ELECTRIC SPRING

Tinglong Pan[1], Xiaobo Lu[1], Zhenlan Dou[2], Weilin Yang[1] and Dezhi Xu[3,4,*]

[1]School of Internet of Things Engineering
Jiangnan University
No. 1800, Lihu Avenue, Wuxi 214122, P. R. China
{ tlpan; wlyang }@jiangnan.edu.cn; 6221915017@stu.jiangnan.edu.cn

[2]State Grid Shanghai Municipal Electric Power Company
No. 677, Jumen Road, Huangpu District, Shanghai 200023, P. R. China
douzhl@sh.sgcc.com.cn

[3]School of Electrical Engineering
[4]Engineering Research Center of Electrical Transport Technology, Ministry of Education
Southeast University
No. 2, Sipailou, Xuanwu District, Nanjing 210096, P. R. China
*Corresponding author: xudezhi@seu.edu.cn

Received December 2024; revised March 2025

Abstract. *Due to the uncertainty of distributed generation, the voltage at the grid side fluctuates, and the non-linearity of electric spring leads to poor control effectiveness of the system. To address these issues, this paper proposes a novel command-filtered backstepping sliding mode control strategy to maintain the stability of the critical load voltage and improve system performance. Firstly, the mathematical model of the microgrid system with a three-phase electric spring is established, which is controlled based on the backstepping method. The accuracy and robustness of the system are enhanced by introducing command filter and sliding mode control, and the stability of the system is verified using Lyapunov stability theory. Through Matlab/Simulink simulation analysis, the stability effect of the TPES on CL voltage and the influence of system parameter changes on the proposed control strategy are studied when voltage fluctuates at the grid side of the distributed generation system. By comparing the proposed control strategy with PI control, CBSMC has faster response speed and lower THD. Furthermore, when the magnitude and characteristics of the component parameters are altered, the CL voltage deviation is suppressed to within 0.36%. Finally, the superiority of the proposed control strategy is verified by experiments using StarSim MT3200 test platform.*

Keywords: Uncertainty of distributed generation, Three-phase electric spring, Command-filtered backstepping, Sliding mode

1. **Introduction.** In recent years, the depletion of non-renewable energy sources such as oil, coupled with the deterioration of the global environment, has led to increased attention towards renewable energy sources like wind and solar power. However, the inherent intermittency and unpredictability of renewable energy sources make power generation challenging to forecast, often resulting in issues such as voltage fluctuations within the grid [1, 2]. Currently, to improve the power quality of microgrids, many scholars have proposed strategies such as optimizing energy scheduling and increasing reactive power compensation in the system [3]. Electric spring (ES) is a new technology for improving power quality [4]. According to the voltage fluctuation range of the load, the load can be

DOI: 10.24507/ijicic.21.04.955

divided into critical load (CL) and non-critical load (NCL). Additionally, ES and NCL in series constitute a smart load (SL), which can bear this part of the voltage fluctuation in the power grid [5].

Since ES was proposed, many different ES topologies with various structures have been studied. ES-1 was the first topology introduced, featuring only capacitors on its DC side, which provides reactive power compensation but has a limited effective operating range [6]. By replacing the DC capacitor of ES-1 with an energy storage device, ES-2 can achieve both active and reactive power compensation, thereby expanding the effective operating range [7]. ES-3 eliminates the NCL and has an even wider effective operating range [8]. Building on ES-2, ES-4 replaces the DC power supply of the inverter with a PWM rectifier, further enhancing the operating range [9]. Among these topologies, ES-2 is the most popular due to its simple structure and ease of control. Its effectiveness in improving power quality in single-phase systems has been verified, leading to the proposal of three-phase electric spring (TPES) based on ES-2 as a solution for addressing voltage fluctuations in three-phase systems. In terms of ES control research, proportional-integral (PI) control remains the main focus. A double closed-loop control strategy for ES is proposed in [10], which enables ES to provide voltage support to the power grid in response to dynamic demands. However, this strategy is associated with high harmonic content in the output voltage, which may not comply with power quality standards in certain extreme scenarios. The δ control strategy introduced in [11] aims to achieve hybrid compensation of active and reactive power. However, this method requires the collection of a significant number of system parameters and places high demands on parameter accuracy. Abrupt changes in parameters may lead to substantial system fluctuations or even instability. A radial chordwise decomposition (RCD) control method is proposed in [12]. The method ensures the stability of CL voltage while enabling independent control of SL power amplitude and phase angle, with reduced dependence on line parameters. To enhance the control effectiveness of the PI controller for ES, fuzzy PI control is proposed in [13]. This method improves voltage stabilization, even when NCL experiences changes at certain time points. However, this approach only accounts for variations in NCL, whereas practical applications involve changes in all system parameters. The criterion and condition for minimizing average power and oscillation power in a three-phase unbalanced system are first introduced in [14]. Three-phase electric spring, using PI control for voltage regulation and power balance, still requires further refinement to improve control accuracy. A novel TPES circuit design is proposed in [15] to enhance the stability and reliability of the power system by providing dynamic compensation for power fluctuations, but the performance of the control strategy is not thoroughly analyzed. In [16], a comprehensive analysis and control strategy is presented to mitigate negative and zero sequence currents in three-phase unbalanced power systems. Simulation and experimental validation on a 3kW hardware device confirm the validity of the new theory and control approach. However, the impact of parameter changes on system robustness is not explored. To address the slow dynamic response inherent in traditional power control methods, direct power control (DPC) is introduced in [17], which enables fast and accurate power tracking. While the paper considers the effects of changes in CL and NCL on system stability, it reports higher THD in CL voltage. A backstepping control strategy using shunt off-grid inverters is proposed in [18], with experimental results demonstrating the robustness, low THD, and superior performance of the strategy. Command filter is introduced in [19, 20] to address the differential expansion problem in backstepping controller.

In this paper, TPES is a typical multivariable and nonlinear system. Current control strategies for TPES suffer from inaccuracies, lack robustness, and are sensitive to circuit parameters. Backstepping control, widely applied in nonlinear systems [21, 22, 23, 24, 25],

has demonstrated significant success in applications such as aircraft and robots [26, 27]. Thus, backstepping control strategy is implemented in the TPES system to achieve stable CL voltage. To further enhance the system's accuracy and robustness, command filter and sliding mode control are integrated [28, 29]. The primary contributions are illustrated in the following.

1) A novel voltage stability control strategy for TPES, based on backstepping method, has been designed. Compared to traditional linear control methods, it demonstrates superior adaptability when addressing complex nonlinear dynamics.

2) In order to eliminate differential expansion and enhance the robustness of the system, command filter and sliding mode control are introduced.

3) The proposed voltage stability control strategy is validated through both qualitative and quantitative analyses, demonstrating strict system stability and examining the impact of changes in system parameters on the control strategy.

The rest of this article is structured as follows. The composition and principle of TPES is introduced in Section 2. Section 3 gives main derivation process and stability proof of CBSMC. In Section 4 and Section 5, simulation and experimental results are given, and analyzed and compared. Section 6 concludes finally.

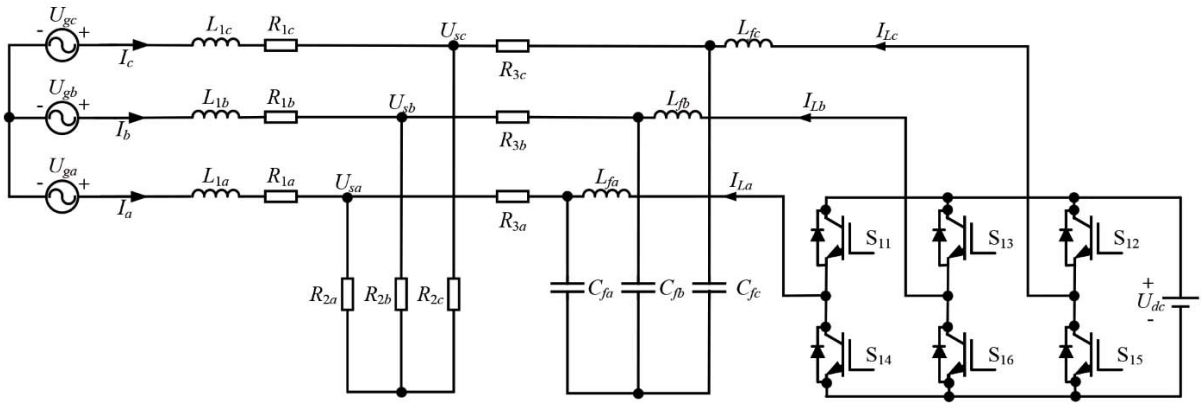

FIGURE 1. Topology of TPES

2. **Principle of Three-Phase Electric Spring.** Figure 1 illustrates the topology of TPES, which consists of a three-phase inverter and an LC low-pass filter. The components L_{fi} and C_{fi} represent the inductance and capacitance of the filter, respectively, where i denotes the phases a, b, and c. The transmission line impedance is represented by R_{1i} and L_{1i}. R_{2i} corresponds to a critical load (CL) where the voltage at both ends must remain stable, while R_{3i} represents a non-critical load (NCL) where the voltage is allowed to fluctuate within a broader range. The grid voltage is denoted by U_{gi}, and the voltage at the point of common coupling (PCC) is represented by U_{si}. The current flowing from the grid to the PCC is denoted by I_i, while I_{Li} refers to the current passing through the inductor L_{fi}. TPES and R_{3i} are connected in series to form a smart load (SL), with SL in parallel with the critical load R_{2i}. When voltage fluctuations occur on the grid side, TPES transfers the voltage fluctuation on CL to NCL and achieves real-time autonomous tracking of the reference voltage value of CL by adjusting the voltage of NCL. Using KCL and KVL, the state equation for TPES in the $\alpha\beta$ coordinate system can be derived:

$$\frac{d}{dt}\begin{bmatrix} I_{L\alpha} \\ I_{L\beta} \end{bmatrix} = -\frac{1}{L_f}\begin{bmatrix} U_{es\alpha} \\ U_{es\beta} \end{bmatrix} + \frac{1}{L_f}\begin{bmatrix} U_{i\alpha} \\ U_{i\beta} \end{bmatrix} \tag{1}$$

$$\frac{d}{dt}\begin{bmatrix} U_{es\alpha} \\ U_{es\beta} \end{bmatrix} = \frac{1}{C_f}\begin{bmatrix} I_{L\alpha} \\ I_{L\beta} \end{bmatrix} + \frac{R_2}{C_f(R_2+R_3)}\begin{bmatrix} I_\alpha \\ I_\beta \end{bmatrix} - \frac{1}{C_f(R_2+R_3)}\begin{bmatrix} U_{es\alpha} \\ U_{es\beta} \end{bmatrix} \tag{2}$$

$$\frac{d}{dt}\begin{bmatrix} I_\alpha \\ I_\beta \end{bmatrix} = -\frac{R_2}{L_1(R_2+R_3)}\begin{bmatrix} U_{es\alpha} \\ U_{es\beta} \end{bmatrix} + \frac{1}{L_1}\begin{bmatrix} U_{g\alpha} \\ U_{g\beta} \end{bmatrix} - \frac{R_1R_2+R_1R_3+R_2R_3}{L_1(R_2+R_3)}\begin{bmatrix} I_\alpha \\ I_\beta \end{bmatrix} \tag{3}$$

$$\begin{bmatrix} U_{s\alpha} \\ U_{s\beta} \end{bmatrix} = \frac{R_2}{R_2+R_3}\begin{bmatrix} U_{es\alpha} \\ U_{es\beta} \end{bmatrix} + \frac{R_2R_3}{R_2+R_3}\begin{bmatrix} I_\alpha \\ I_\beta \end{bmatrix} \tag{4}$$

3. Proposed Controller Design.

3.1. **Virtual controller design.** According to the principle of the inverter, the relationship between the output voltage U_i of the three-phase inverter and the PWM modulated signal can be written as $U_i = U_{dc} * m/2$. Therefore, Formula (1) can be rewritten as

$$\frac{d}{dt}\begin{bmatrix} I_{Ld} \\ I_{Lq} \end{bmatrix} = \begin{bmatrix} \omega I_{Lq} \\ -\omega I_{Ld} \end{bmatrix} - \frac{1}{L_f}\begin{bmatrix} U_{esd} \\ U_{esq} \end{bmatrix} + \frac{1}{2L_f}\begin{bmatrix} U_{dc}m_d \\ U_{dc}m_q \end{bmatrix} \tag{5}$$

The error between the critical load voltage and the reference voltage can be defined as

$$\begin{aligned} e_1 &= U_{sd} - U_{srefd} \\ e_2 &= U_{sq} - U_{srefq} \end{aligned} \tag{6}$$

Derivation of Equation (6) gives

$$\begin{aligned} \dot{e}_1 &= \dot{U}_{sd} - \dot{U}_{srefd} \\ \dot{e}_2 &= \dot{U}_{sq} - \dot{U}_{srefq} \end{aligned} \tag{7}$$

The Lyapunov function can be defined as

$$\begin{aligned} V_1 &= \frac{1}{2}{e_1}^2 \\ V_2 &= \frac{1}{2}{e_2}^2 \end{aligned} \tag{8}$$

By taking the derivative of Equation (8) and substituting Equation (7), we get

$$\begin{aligned} \dot{V}_1 &= e_1\dot{e}_1 = e_1\left(\dot{U}_{sd} - \dot{U}_{srefd}\right) = -k_1{e_1}^2 + e_1\left(k_1e_1 + \dot{U}_{sd} - \dot{U}_{srefd}\right) \\ \dot{V}_2 &= e_2\dot{e}_2 = e_2\left(\dot{U}_{sq} - \dot{U}_{srefq}\right) = -k_2{e_2}^2 + e_2\left(k_2e_2 + \dot{U}_{sq} - \dot{U}_{srefq}\right) \end{aligned} \tag{9}$$

Taking the derivative of Equation (4), substituting Equations (2) and (3), yields dU_{sdq}/dt in the dq coordinate system

$$\begin{aligned} \frac{d}{dt}\begin{bmatrix} U_{sd} \\ U_{sq} \end{bmatrix} = {} & \begin{bmatrix} \omega U_{sq} \\ -\omega U_{sd} \end{bmatrix} + \frac{R_2}{C_f(R_2+R_3)}\begin{bmatrix} I_{Ld} \\ I_{Lq} \end{bmatrix} - \frac{R_2}{C_f(R_2+R_3)^2}\begin{bmatrix} U_{esd} \\ U_{esq} \end{bmatrix} \\ & + \frac{{R_2}^2}{C_f(R_2+R_3)^2}\begin{bmatrix} I_d \\ I_q \end{bmatrix} - \frac{{R_2}^2R_3}{L_1(R_2+R_3)^2}\begin{bmatrix} U_{esd} \\ U_{esq} \end{bmatrix} + \frac{R_2R_3}{L_1(R_2+R_3)}\begin{bmatrix} U_{gd} \\ U_{gq} \end{bmatrix} \\ & - \frac{(R_2R_3)(R_1R_2+R_1R_3+R_2R_3)}{L_1(R_2+R_3)^2}\begin{bmatrix} I_d \\ I_q \end{bmatrix} \end{aligned} \tag{10}$$

According to the Lyapunov stability law, for the system to be stable, $\dot{V}_1 \le 0$ and $\dot{V}_2 \le 0$ must be satisfied, so $k_1e_1 + \dot{U}_{sd} - \dot{U}_{srefd} = 0$ and $k_2e_2 + \dot{U}_{sq} - \dot{U}_{srefq} = 0$ are satisfied. Virtual controllers ${I_{Ld}}^d$ and ${I_{Lq}}^d$ can get the input current of the inverter as follows

$$\begin{aligned} & {I_{Ld}}^d \\ &= \left[\frac{C_fR_3(R_1R_2+R_1R_3+R_2R_3)}{L_1(R_2+R_3)} - \frac{R_2}{R_2+R_3}\right]I_d + \left[\frac{1}{R_2+R_3} + \frac{C_fR_2R_3}{L_1(R_2+R_3)}\right]U_{esd} \end{aligned}$$

$$
\begin{aligned}
&-\frac{C_f(R_2+R_3)\omega}{R_2}U_{sq}-\frac{C_fR_3}{L_1}U_{gd}-\frac{C_f(R_2+R_3)}{R_2}\left(k_1e_1-\dot{U}_{srefd}\right)\\
&{I_{Lq}}^d\\
&=\left[\frac{C_fR_3(R_1R_2+R_1R_3+R_2R_3)}{L_1(R_2+R_3)}-\frac{R_2}{R_2+R_3}\right]I_q+\left[\frac{1}{R_2+R_3}+\frac{C_fR_2R_3}{L_1(R_2+R_3)}\right]U_{esq}\\
&+\frac{C_f(R_2+R_3)\omega}{R_2}U_{sd}-\frac{C_fR_3}{L_1}U_{gq}-\frac{C_f(R_2+R_3)}{R_2}\left(k_2e_2-\dot{U}_{srefq}\right)
\end{aligned}
\tag{11}
$$

In high-order nonlinear systems, the virtual controller will be repeatedly differentiated when designing the backstepping controller. This can easily cause the differential expansion problem, which affects the control performance of the virtual controller on the system. To address this issue, various approaches such as adaptive control, interference observers, and command filter are commonly employed. In this paper, the primary motivation for selecting command filter lies in its simplicity and effectiveness. By adjusting the bandwidth and damping coefficient appropriately, the command filter can smooth the control command, mitigate the impact of high-frequency noise, and offer ease of implementation. This makes it particularly suitable for applications with high complexity and stringent real-time requirements. Although adaptive control and interference observers exhibit strong theoretical performance, they often require more intricate models and parameter tuning, which can increase both the complexity and computational load of the implementation. This is particularly challenging in practical scenarios, where parameter uncertainties and dynamic system changes may arise. The structure diagram of the command filter is shown in Figure 2.

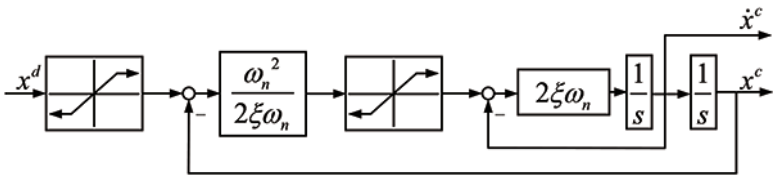

FIGURE 2. Command filter

In this paper, x^d represents the input signal of the command filter, which is specifically denoted as ${I_{Ldq}}^d$. The output signal and its derivative of the command filter are represented by x^c and $\dot{x}^c$, respectively, and are specifically expressed as ${I_{Ldq}}^c$ and ${\dot{I}_{Ldq}}^c$ in the context of this study. ω_n and ξ are the bandwidth and damping of the command filter, respectively, and the equation of state of the command filter is

$$
\begin{bmatrix} \dot{q}_1 \\ \dot{q}_2 \end{bmatrix} = \begin{bmatrix} q_2 \\ 2\xi\omega_n\left[S_R\left(\dfrac{{\omega_n}^2}{2\xi\omega_n}\right)(S_M(u)-q_1)-q_2\right] \end{bmatrix}
\tag{12}
$$

where,

$$
\begin{bmatrix} q_1 \\ q_2 \end{bmatrix} = \begin{bmatrix} x^c \\ \dot{x}^c \end{bmatrix}, \quad u = x^d
\tag{13}
$$

And S_R and S_M represent the rate and magnitude limit, respectively.

In order to achieve the control goal, the command filter needs to reduce the error of the input signal x^d and the output signal x^c as much as possible. At this time, as long as the bandwidth ω_n inside the command filter is as large as possible, the error of x^d and x^c can be close to 0.

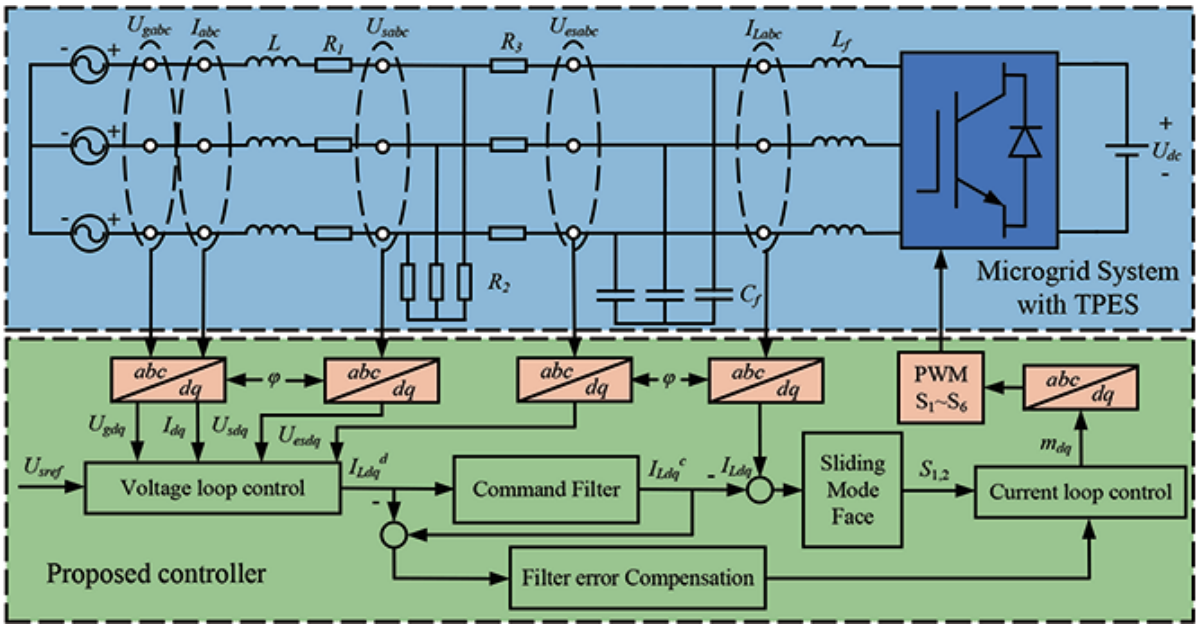

FIGURE 3. Reverse sliding mode control block diagram of TPES with command filter

Figure 3 shows the backstepping sliding mode control block diagram of TPES with command filter. In order to compensate the filtering error of the command filter, the error amount is redefined as

$$\begin{aligned} \bar{e}_1 &= e_1 - \varepsilon_1 \\ \bar{e}_2 &= e_2 - \varepsilon_2 \end{aligned} \tag{14}$$

where, ε_1 and ε_2 are error compensation signals of the command filter, and their derivatives are designed as shown in the formula.

$$\begin{aligned} \dot{\varepsilon}_1 &= -k_1\varepsilon_1 + \frac{R_2}{C_f(R_2+R_3)}\left({I_{Ld}}^c - {I_{Ld}}^d\right) \\ \dot{\varepsilon}_2 &= -k_2\varepsilon_2 + \frac{R_2}{C_f(R_2+R_3)}\left({I_{Lq}}^c - {I_{Lq}}^d\right) \end{aligned} \tag{15}$$

The output inverter current error is defined as

$$\begin{aligned} e_3 &= I_{Ld} - {I_{Ld}}^c \\ e_4 &= I_{Lq} - {I_{Lq}}^c \end{aligned} \tag{16}$$

For convenience of later calculation, $\dot{\bar{e}}_{1,2}$ can be calculated as follows according to Equations (11) and (15)

$$\begin{aligned} \dot{\bar{e}}_1 &= \dot{e}_1 - \dot{\varepsilon}_1 \\ &= \dot{U}_{sd} - \dot{U}_{srefd} + k_1\varepsilon_1 - \frac{R_2}{C_f(R_2+R_3)}\left({I_{Ld}}^c - {I_{Ld}}^d\right) \\ &= -k_1\bar{e}_1 + \frac{R_2}{C_f(R_2+R_3)}e_3 \\ \dot{\bar{e}}_2 &= \dot{e}_2 - \dot{\varepsilon}_2 \\ &= \dot{U}_{sq} - \dot{U}_{srefq} + k_2\varepsilon_2 - \frac{R_2}{C_f(R_2+R_3)}\left({I_{Lq}}^c - {I_{Lq}}^d\right) \end{aligned}$$

$$= -k_2\bar{e}_2 + \frac{R_2}{C_f(R_2+R_3)}e_4 \tag{17}$$

The dq axis controller adopts a first-order sliding mode, which is as follows

$$\begin{aligned} S_1 &= e_3 \\ S_2 &= e_4 \end{aligned} \tag{18}$$

To keep the entire system stable, the Lyapunov function is redefined as

$$V_3 = \frac{1}{2}\left(\bar{e}_1^2 + \bar{e}_2^2 + {S_1}^2 + {S_2}^2\right) \tag{19}$$

By differentiating it, we can get

$$\dot{V}_3 = \bar{e}_1\dot{\bar{e}}_1 + \bar{e}_2\dot{\bar{e}}_2 + S_1\dot{S}_1 + S_2\dot{S}_2 \tag{20}$$

The derivatives of the sliding mode surfaces S_1 and S_2 are shown as follows

$$\begin{aligned} \dot{S}_1 = \dot{e}_3 &= \dot{I}_{Ld} - {\dot{I}_{Ld}}^c = \omega I_{Lq} - \frac{U_{esd}}{L_f} + \frac{U_{dc}m_d}{2L_f} - {\dot{I}_{Ld}}^c \\ \dot{S}_2 = \dot{e}_4 &= \dot{I}_{Lq} - {\dot{I}_{Lq}}^c = -\omega I_{Ld} - \frac{U_{esq}}{L_f} + \frac{U_{dc}m_q}{2L_f} - {\dot{I}_{Lq}}^c \end{aligned} \tag{21}$$

By substituting Equations (17) and (21) into Equation (20), the following conclusions can be drawn

$$\begin{aligned} \dot{V}_3 = -k_1\bar{e}_1^2 - k_2\bar{e}_2^2 &+ S_1\left[\frac{R_2\bar{e}_1}{C_f(R_2+R_3)} + \omega I_{Lq} - \frac{U_{esd}}{L_f} + \frac{U_{dc}m_d}{2L_f} - {\dot{I}_{Ld}}^c\right] \\ &+ S_2\left[\frac{R_2\bar{e}_2}{C_f(R_2+R_3)} - \omega I_{Ld} - \frac{U_{esd}}{L_f} + \frac{U_{dc}m_q}{2L_f} - {\dot{I}_{Lq}}^c\right] \end{aligned} \tag{22}$$

In order to ensure the global asymptotic stability of the entire TPES, the sliding mode control algorithm must guarantee $\dot{V}_3 \leq 0$, so it can be obtained as follows

$$\begin{aligned} -k_3 Sat(S_1) &= \frac{R_2\bar{e}_1}{C_f(R_2+R_3)} + \omega I_{Lq} - \frac{U_{esd}}{L_f} + \frac{U_{dc}m_d}{2L_f} - {\dot{I}_{Ld}}^c \\ -k_4 Sat(S_2) &= \frac{R_2\bar{e}_2}{C_f(R_2+R_3)} - \omega I_{Ld} - \frac{U_{esq}}{L_f} + \frac{U_{dc}m_q}{2L_f} - {\dot{I}_{Lq}}^c \end{aligned} \tag{23}$$

where k_3 and k_4 are adjustable parameters, and the function Sat denotes the saturation function, defined as follows

$$Sat(S) = \begin{cases} 1, & S > \sigma \\ S/\sigma, & |S| \leq \sigma \\ -1, & S < -\sigma \end{cases} \tag{24}$$

where σ represents the sliding layer, ranging from 0 to 0.5. Consequently, the control rates m_d and m_q can be determined as follows

$$\begin{aligned} m_d &= \frac{2L_f}{U_{dc}}\left[-\frac{R_2}{C_f(R_2+R_3)}\bar{e}_1 - \omega I_{Lq} + \frac{U_{esd}}{L_f} - k_3 Sat(S_1) + {\dot{I}_{Ld}}^c\right] \\ m_q &= \frac{2L_f}{U_{dc}}\left[-\frac{R_2}{C_f(R_2+R_3)}\bar{e}_2 + \omega I_{Ld} + \frac{U_{esq}}{L_f} - k_4 Sat(S_2) + {\dot{I}_{Lq}}^c\right] \end{aligned} \tag{25}$$

3.2. **Stability analysis.** In the process of designing the current and control rate of the virtual controller, the Lyapunov function is employed to ensure system stability. The coefficients k_1, k_2, k_3 and k_4 are constants greater than 0. As can be seen from Equations (8) and (19), the three Lyapunov functions constructed are all positive definite functions.

The derivation of the aforementioned three Lyapunov functions is conducted, and Equations (11) and (25) for the designed virtual controller and control rate are substituted into Equations (9) and (22), respectively.

$$\dot{V}_1 = e_1\dot{e}_1 = -k_1{e_1}^2 \leq 0$$
$$\dot{V}_2 = e_2\dot{e}_2 = -k_2{e_2}^2 \leq 0$$
$$\dot{V}_3 = \bar{e}_1\dot{\bar{e}}_1 + \bar{e}_2\dot{\bar{e}}_2 + S_1\dot{S}_1 + S_2\dot{S}_2 = -k_1\bar{e}_1^2 - k_2\bar{e}_2^2 - k_3S_1Sat(S_1) - k_4S_2Sat(S_2) \leq 0 \quad (26)$$

According to Lyapunov stability theory, the designed virtual controller current ${I_{Ld}}^d$, ${I_{Lq}}^d$ and control rate m_d, m_q are asymptotically stable at the origin, so as to keep the whole system stable.

4. **Simulation and Result Analysis.** To verify the feasibility and superiority of the proposed CBSMC, simulations were conducted in the MATLAB/Simulink environment. The parameters of components in the TPES simulation model are detailed in Table 1.

Table 1. System model parameter

Parameters	Value
Grid frequency (f)	50 Hz
Reference voltage (U_{sref})	220 V
DC bus voltage (U_{dc})	800 V
Line resistance (R_1)	0.1 Ω
Line inductance (L_1)	0.02 H
Critical load (R_2)	100 Ω
Non-critical load (R_3)	50 Ω
Inductance of filter (L_f)	50 mH
Capacitance of filter (C_f)	50 μF
Switching frequency (f_s)	10 kHz
k_1	300
k_2	10
k_3	50000
k_4	8000

To assess the stabilizing effect of TPES on CL voltage during drops in grid-side voltage in new energy power generation systems, simulations were conducted over a duration of 2 s. The grid-side voltage is rated at 311 V from 0 to 0.5 s, during which both CL and NCL voltages remain stable at 311 V. At 0.5 s, the grid-side voltage drops to 0.9 p.u. Without TPES, both CL and NCL voltages show significant drops. TPES is connected to the microgrid at 0.7 s to compensate for the CL voltage. The simulation results are depicted in Figure 4, where 4(a) shows the voltage waveform output by the TPES, 4(b) displays the NCL voltage waveform, 4(c) shows the CL voltage waveform, and 4(d) illustrates the RMS waveform of the CL voltage. Figures 4(a) and 4(b) illustrate that when TPES is connected at 0.7 s, the proposed control strategy effectively transfers voltage fluctuations from CL to NCL. Figures 4(c) and 4(d) demonstrate that the CL voltage stabilizes around 0.77 s with the proposed strategy, whereas with the PI control strategy, stabilization occurs around 1.15 s with significant overshoot. The response speed of the proposed control strategy is

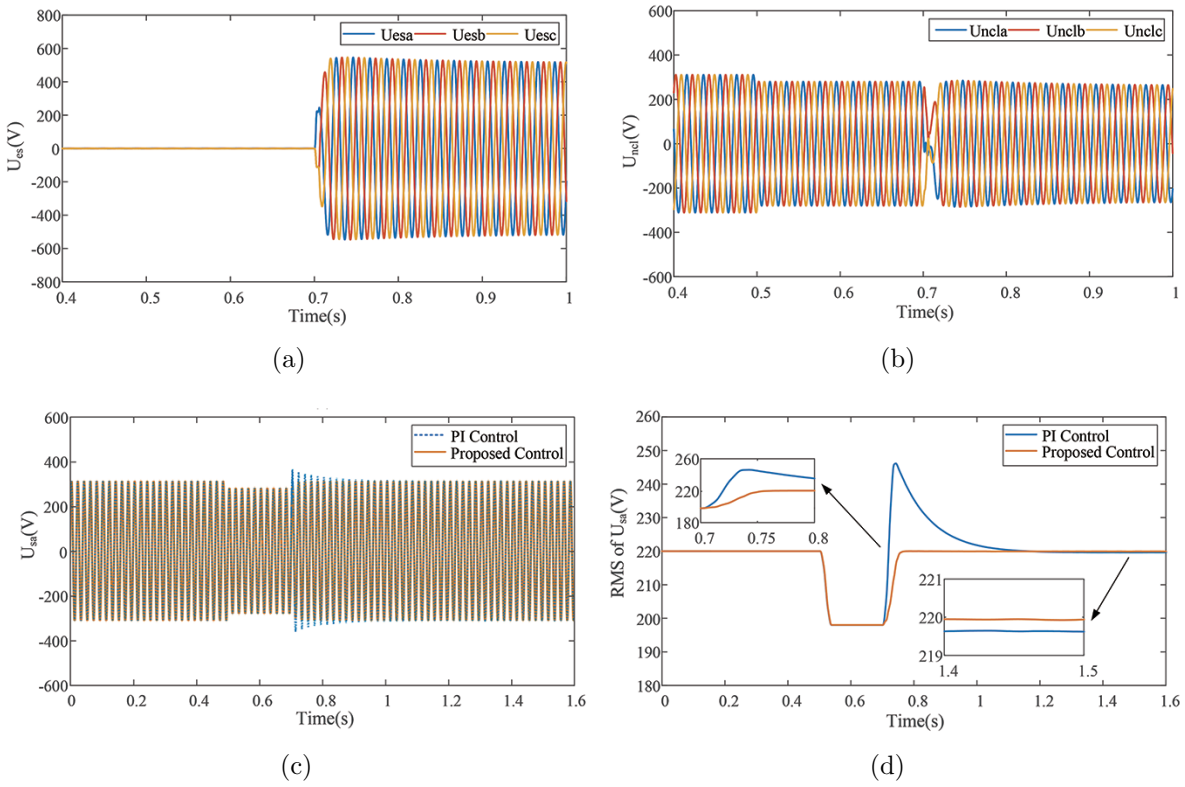

FIGURE 4. Simulation results under the method of CBSMC: (a) TPES voltage waveform; (b) NCL voltage waveform; (c) CL voltage waveform; (d) RMS waveform of CL voltage

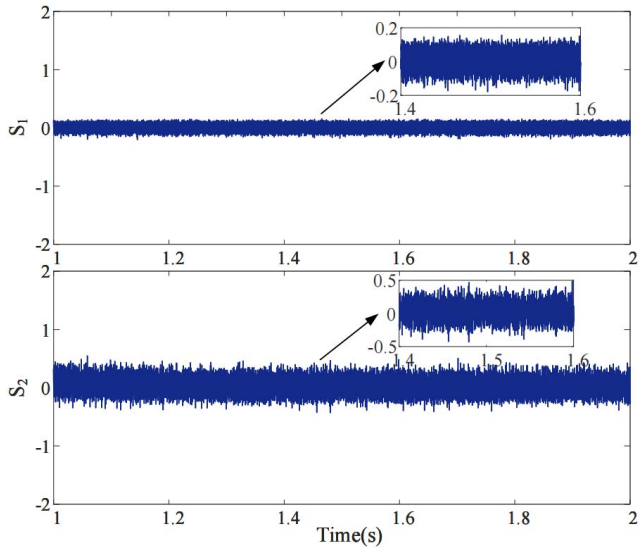

FIGURE 5. The responses of sliding mode surfaces S_1 and S_2

0.38 s faster than that of PI control, and there is no obvious overshoot in the control process. Furthermore, at stable CL voltages, the steady-state error is approximately 0.4 V under PI control compared to about 0.05 V under the proposed strategy, indicating significantly reduced error with the latter.

The sliding modes and are depicted in Figure 5. From the figure, it is evident that the controller designed in this study achieves convergence of the control object to the sliding

mode planes S_1 and S_2. The jitter suppression within sliding mode plane S_1 ranges between -0.2 and 0.2, while within sliding mode plane S_2, it ranges between -0.5 and 0.5.

Figure 6 shows the total harmonic distortion (THD) under two control strategies. Throughout the simulation, the THD of the CL voltage waveform under the PI control strategy is 0.83% with an amplitude of 310.6 V. In contrast, under CBSMC, the THD of the CL voltage waveform is reduced to 0.06% with an amplitude of 310.9 V, indicating significantly lower waveform distortion.

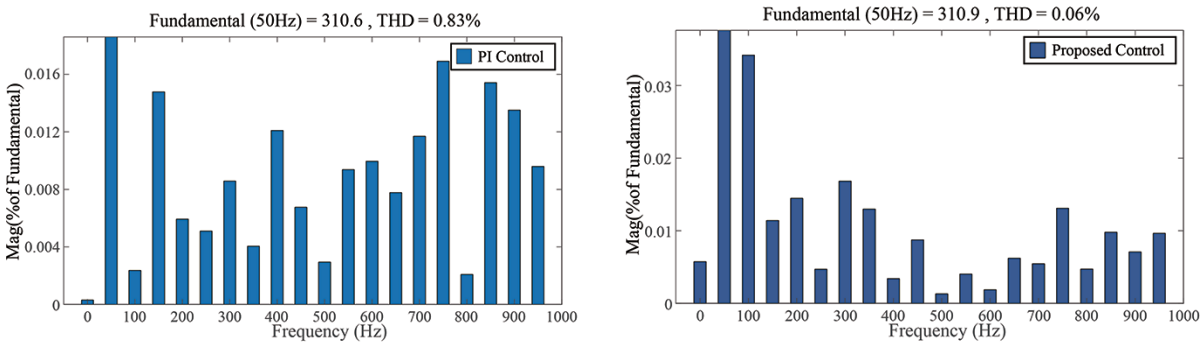

(a) (b)

FIGURE 6. THD of CL voltage under two control strategies: (a) THD in the PI controller; (b) THD in the proposed controller

Therefore, as shown in Table 2, compared with PI control, the proposed control strategy has smaller overshoot, faster response speed, lower THD, smaller steady-state error, and overall superior control effect.

TABLE 2. Comparison of control performance between PI and CBSMC

Control strategy	Response time	Steady-state error	THD
PI	0.45 s	0.4 V	0.83%
CBSMC	0.07 s	0.05 V	0.06%

To assess the impact of system parameters on the proposed control strategy, sensitivity analysis is conducted in this section. The voltage fluctuation at the simulated network side, detailed in Section 3.1, and the parameters listed in Table 1 remain unchanged, with variations applied solely to the parameters of interest in the study. Figure 7 illustrates the impact of line resistance, line inductance, CL value, and NCL value on the effective value of CL voltage. Simulation results indicate that CBSMC keeps CL voltage stable around 220 V despite variations in system parameters. Figures 7(a) and 7(b) demonstrate that line resistance and inductance exert minimal influence on CL voltage. In contrast, Figures 7(c) and 7(d) reveal significant sensitivity of CL voltage to changes in NCL resistance and CL resistance. The maximum voltage deviation is approximately 0.6 V with a deviation rate of about 0.27%, suggesting that CBSMC exhibits low sensitivity to system parameters.

In addition to analyzing the influence of parameter values on the control strategy's effectiveness, this study investigates the impact of changes in CL and NCL properties on final voltage stability. CL and NCL transition from their initial resistive states of 100 Ω and 50 Ω to 100+j0.01 Ω and 50+j0.01 Ω, respectively. Figure 8 illustrates the voltage waveform response to these changes from pure resistive loads to complex impedances. The results indicate that variations in CL properties have minimal effect on voltage stability. Conversely, changes in NCL properties significantly affect voltage stability, causing the

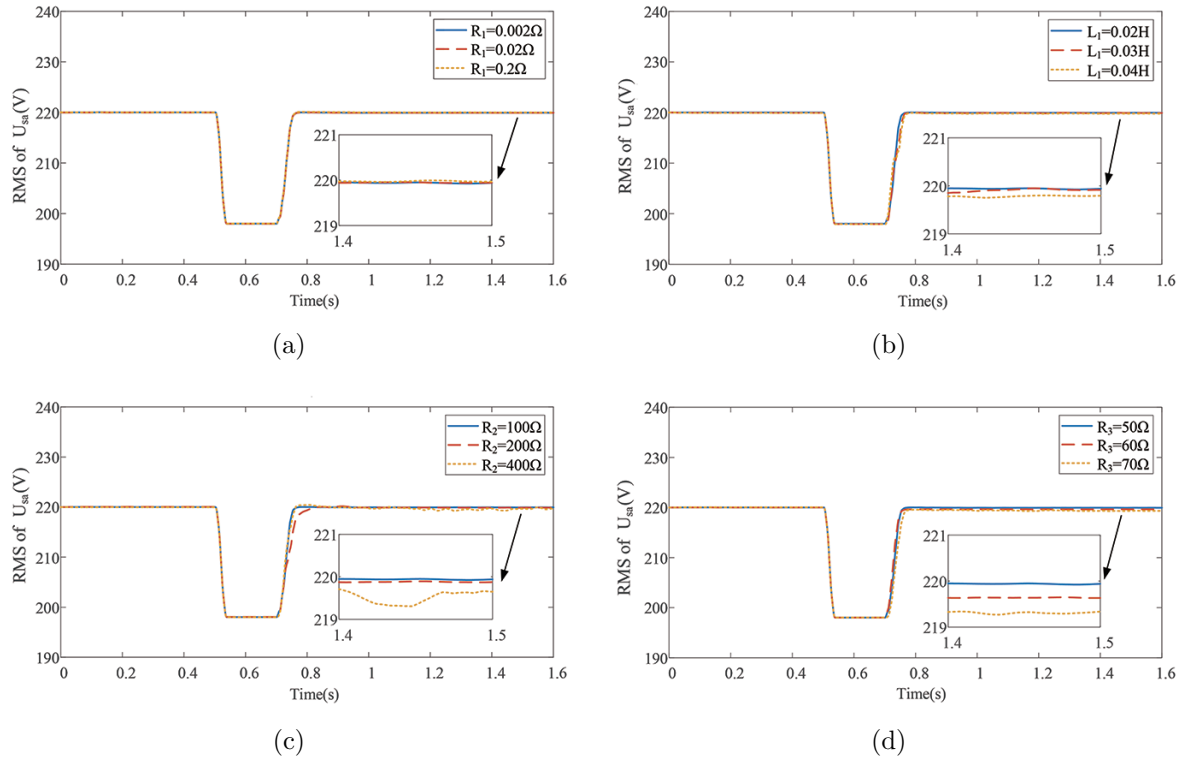

FIGURE 7. Results of sensitivity analysis of system parameter value: (a) Influence of line resistance value; (b) influence of line inductance value; (c) influence of CL resistance value; (d) influence of NCL resistance value

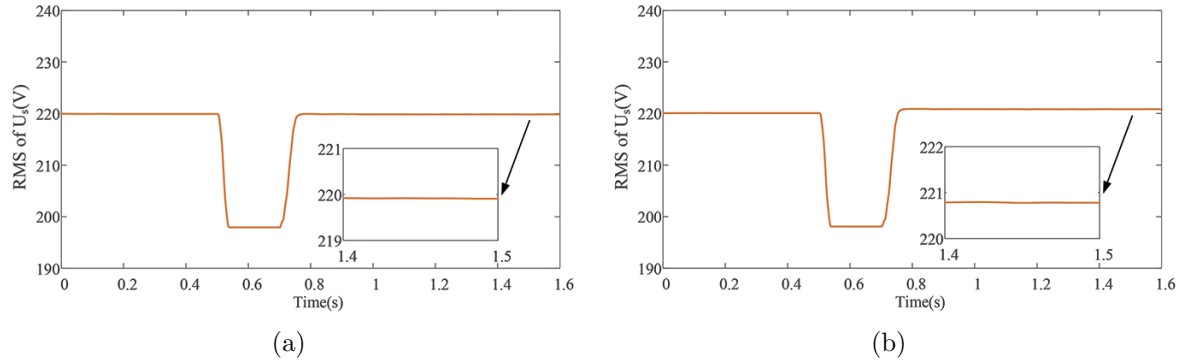

FIGURE 8. Results of sensitivity analysis of system element properties: (a) Influence of CL property change; (b) influence of NCL property change

actual voltage to exceed the reference voltage. Nevertheless, the CL voltage deviation is 0.8 V, with a deviation rate of approximately 0.36%, which meets the national power quality standard. These findings underscore the proposed control strategy's robustness against variations in load properties.

5. **Experiment and Result Analysis.**

5.1. **Introduction of experimental platform.** To further substantiate the effectiveness of CBSMC, a series of real-time simulation experiments were conducted using the StarSim MT3200 test platform. The experimental platform is shown in Figure 9. The experimental device is mainly composed of the MT3200 and the host computer, in which the

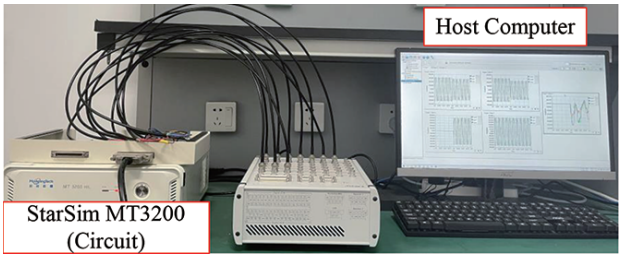

FIGURE 9. Experiment platform based on StarSim HIL

MT3200 uses a dual-core ARM Cortex-A9 processor, the main frequency is up to 1 GHz, and the built-in Xilinx ZYNQ-7100 series FPGA chip has rich logic resources and high-speed I/O interface. In addition, StarSim HIL is an upper computer software that works with the MT3200 to interconnect the MT3200 with the host to build an FPGA-based hardware-in-the-loop system.

5.2. **Experimental step.** In the hardware-in-the-loop experiment, the inverter and the corresponding filter circuit, line impedance and load resistance were built in Simulink, and the circuit model was imported into the upper computer software StarSim HIL of MT3200 after completion. In StarSim HIL, the built main circuit model is assigned to the FPGA of the MT3200. The control module is first compiled by Simulink and then downloaded into the CPU as the controller. After all modules have been successfully compiled and allocated, the interface connection between the CPU and FPGA needs to be completed in StarSim HIL. Finally, the experimental results can be recorded and analyzed through the observation window of StarSim HIL. The parameters used in the experiment are shown in Table 3.

TABLE 3. Experimental parameter

Parameters	Value
DC bus voltage (U_{dc})	800 V
Line resistance (R_1)	0.01 Ω
Line inductance (L_1)	0.02 H
Critical load (R_2)	100 Ω
Non-critical load (R_3)	50 Ω
Inductance of filter (L_f)	6 mH
Capacitance of filter (C_f)	50 μF

5.3. **Result analysis.** The experimental waveforms of TPES under the CBSMC control strategy are depicted in Figure 10 and Figure 11. During the experiment, the voltage reference on the network side remained unchanged from 0 to 0.5 s. However, after 0.5 s, there was a significant drop in the network voltage. U_g in Figure 10 drops to 0.95 p.u. and U_g in Figure 11 drops to 0.9 p.u. Concurrently, the voltage of the CL also decreased notably. TPES accesses the PCC point at 0.7 s and implements corresponding compensation measures for U_s through CBSMC. The TPES system can rapidly adjust its output to manage voltage fluctuations on the network side efficiently using the sliding mode control strategy. Simultaneously, the command filter ensures a smoother and more accurate voltage compensation process, preventing overshoot or oscillation typically caused by transient responses.

The experimental results demonstrate that the proposed CBSMC exhibits strong robustness and rapid response capability. It efficiently compensates and adjusts to voltage

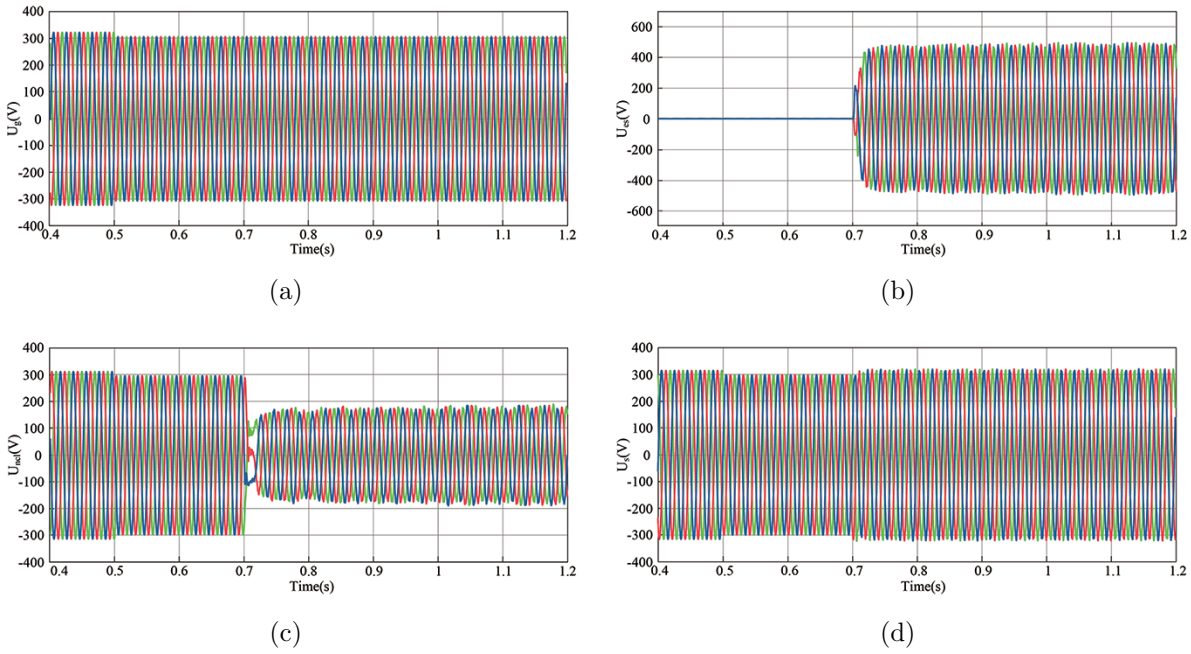

FIGURE 10. Experimental results of CBSMC strategy in U_g small drop: (a) Grid voltage change waveform; (b) TPES voltage change waveform; (c) NCL voltage change waveform; (d) CL voltage change waveform

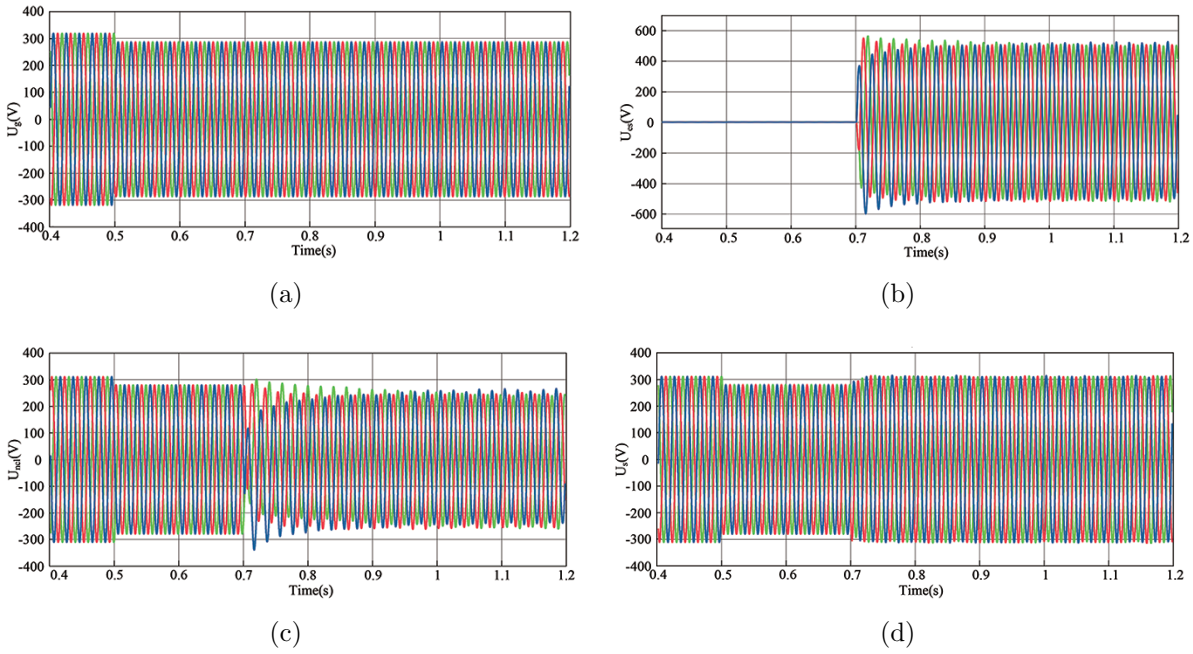

FIGURE 11. Experimental results of CBSMC strategy in U_g large drop: (a) Grid voltage change waveform; (b) TPES voltage change waveform; (c) NCL voltage change waveform; (d) CL voltage change waveform

fluctuations on the network side, ensuring stable voltage and reliable system operation. By employing this control strategy, the system achieves quick restoration of voltage stability and effective suppression of fluctuations, thereby enhancing power quality and system reliability.

6. **Conclusion.** This paper addresses the limitations of traditional ES voltage control methods by proposing a novel CBSMC. This approach significantly enhances dynamic voltage control response, reduces overshoot during control processes, and minimizes steady-state errors upon reaching stability. Building upon the state space equation of TPES, this study introduces backstepping control. To mitigate differential expansion issues in the backstepping controller design, the command filter is incorporated, bolstering system robustness through sliding mode control. Simulation and experimental results indicate that compared to PI control strategies, the proposed method achieves faster stabilization of CL voltage with reduced overshoot and steady-state error. Furthermore, FFT analysis reveals lower harmonic content and waveform distortion rates, highlighting the superior stability effect on CL voltage afforded by the proposed strategy. Sensitivity analysis of system parameters demonstrates that changes in CL and NCL values exert significant influence, yet the system stabilizes around 220 V with maximum deviations of 0.8 V and a deviation rate of 0.36%. Although the proposed control strategy demonstrates excellent stability and robustness, its substantial computational requirements present a significant challenge for hardware implementation in practical applications. Furthermore, in many real-world scenarios, most of the model parameters remain unknown. To address these issues, future work could explore the integration of adaptive algorithms, which would enable the online estimation of uncertain parameters within TPES systems.

Acknowledgements. This work is partially supported by the National Natural Science Foundation of China (Grant No. 62222307, No. 61973140) and the Natural Science Foundation of Jiangsu Province (Grant No. BK20211235). The authors also appreciatively acknowledge the helpful suggestions and comments of the reviewers, which have enhanced the presentation.

REFERENCES

[1] H. Hu, Y. Zhou, X. Li and K. Lei, Low-frequency oscillation in electric railway depot: A comprehensive review, *IEEE Transactions on Power Electronics*, vol.36, no.1, pp.295-314, 2020.

[2] Y. Guo, Q. Wang and J. Yu, Assessment of voltage fluctuations based on wind power fluctuation characteristics, *The 8th Renewable Power Generation Conference (RPG 2019)*, pp.1-6, 2019.

[3] P. Zou, Q. Chen, Q. Xia, G. He and C. Kang, Evaluating the contribution of energy storages to support large-scale renewable generation in joint energy and ancillary service markets, *IEEE Transactions on Sustainable Energy*, vol.7, no.2, pp.808-818, 2015.

[4] S. Y. Hui, C. K. Lee and F. F. Wu, Electric springs – A new smart grid technology, *IEEE Transactions on Smart Grid*, vol.3, no.3, pp.1552-1561, 2012.

[5] J. Soni and S. K. Panda, Electric spring for voltage and power stability and power factor correction, *IEEE Transactions on Industry Applications*, vol.53, no.4, pp.3871-3879, 2017.

[6] C. K. Lee, B. Chaudhuri and S. Y. Hui, Hardware and control implementation of electric springs for stabilizing future smart grid with intermittent renewable energy sources, *IEEE Journal of Emerging and Selected Topics in Power Electronics*, vol.1, no.1, pp.18-27, 2013.

[7] S.-C. Tan, C. K. Lee and S. Hui, General steady-state analysis and control principle of electric springs with active and reactive power compensations, *IEEE Transactions on Power Electronics*, vol.28, no.8, pp.3958-3969, 2012.

[8] D. Qiu, C. Yuan, B. Zhang, M. Ke, Y. Chen and F. Xie, An improved electric spring topology based on LCL filter, *IEEE Transactions on Power Electronics*, vol.37, no.5, pp.5984-5994, 2021.

[9] Z. Akhtar, B. Chaudhuri and S. Y. R. Hui, Smart loads for voltage control in distribution networks, *IEEE Transactions on Smart Grid*, vol.8, no.2, pp.937-946, 2015.

[10] Y. Shuo, S.-C. Tan, C. Lee and S. R. Hui, Electric spring for power quality improvement, *2014 IEEE Applied Power Electronics Conference and Exposition (APEC 2014)*, pp.2140-2147, 2014.

[11] Q. Wang, M. Cheng, Z. Chen and Z. Wang, Steady-state analysis of electric springs with a novel δ control, *IEEE Transactions on Power Electronics*, vol.30, no.12, pp.7159-7169, 2015.

[12] K.-T. Mok, S.-C. Tan and S. R. Hui, Decoupled power angle and voltage control of electric springs, *IEEE Transactions on Power Electronics*, vol.31, no.2, pp.1216-1229, 2016.

[13] G. Ma, G. Xu, Y. Chen and R. Ju, Voltage stability control method of electric springs based on adaptive PI controller, *International Journal of Electrical Power & Energy Systems*, vol.95, pp.202-212, 2018.

[14] S. Yan, M.-H. Wang, T.-B. Yang, S.-C. Tan, B. Chaudhuri and S. R. Hui, Achieving multiple functions of three-phase electric springs in unbalanced three-phase power systems using the instantaneous power theory, *IEEE Transactions on Power Electronics*, vol.33, no.7, pp.5784-5795, 2017.

[15] S. Yan, S.-C. Tan, C.-K. Lee, B. Chaudhuri and S. R. Hui, Electric springs for reducing power imbalance in three-phase power systems, *IEEE Transactions on Power Electronics*, vol.30, no.7, pp.3601-3609, 2015.

[16] K.-T. Mok, S.-S. Ho, S.-C. Tan and S. Hui, A comprehensive analysis and control strategy for nullifying negative-and zero-sequence currents in an unbalanced three-phase power system using electric springs, *IEEE Transactions on Power Electronics*, vol.32, no.10, pp.7635-7650, 2016.

[17] Q. Wang, Z. Ding, M. Cheng, F. Deng and G. Buja, Direct power control of three-phase electric springs, *IEEE Transactions on Industrial Electronics*, vol.69, no.12, pp.13033-13044, 2021.

[18] R.-J. Wai, C.-Y. Lin, W.-C. Wu and H.-N. Huang, Design of backstepping control for high-performance inverter with stand-alone and grid-connected power-supply modes, *IET Power Electronics*, vol.6, no.4, pp.752-762, 2013.

[19] Q. Miao, K. Zhang and B. Jiang, Fixed-time collision-free fault-tolerant formation control of multi-uavs under actuator faults, *IEEE Transactions on Cybernetics*, 2024.

[20] F. Fang, K. Zhang, W. Cheng and B. Jiang, Distributed finite-time fault-tolerant control based on command filtered backstepping for multiple fixed-wing unmanned aerial vehicles, *International Conference on Guidance, Navigation and Control*, pp.1425-1435, 2022.

[21] L. Zhao, J. Yu and Q.-G. Wang, Finite-time tracking control for nonlinear systems via adaptive neural output feedback and command filtered backstepping, *IEEE Transactions on Neural Networks and Learning Systems*, vol.32, no.4, pp.1474-1485, 2020.

[22] Y. Pan, H. Wang, X. Li and H. Yu, Adaptive command-filtered backstepping control of robot arms with compliant actuators, *IEEE Transactions on Control Systems Technology*, vol.26, no.3, pp.1149-1156, 2017.

[23] H. Wang, S. Kang and Z. Feng, Finite-time adaptive fuzzy command filtered backstepping control for a class of nonlinear systems, *International Journal of Fuzzy Systems*, vol.21, no.8, pp.2575-2587, 2019.

[24] L. Zhao, J. Yu, C. Lin and Y. Ma, Adaptive neural consensus tracking for nonlinear multiagent systems using finite-time command filtered backstepping, *IEEE Transactions on Systems, Man, and Cybernetics: Systems*, vol.48, no.11, pp.2003-2012, 2017.

[25] S. Liu, B. Jiang, Z. Mao and S. X. Ding, Adaptive backstepping based fault-tolerant control for high-speed trains with actuator faults, *International Journal of Control, Automation and Systems*, vol.17, no.6, pp.1408-1420, 2019.

[26] K. Liu and R. Wang, Antisaturation command filtered backstepping control-based disturbance rejection for a quadarotor UAV, *IEEE Transactions on Circuits and Systems II: Express Briefs*, vol.68, no.12, pp.3577-3581, 2021.

[27] S. Fan, H. Liu, S. Tian and P. Gu, Observer-based fixed-time output feedback control for flexible-joint manipulators via improved command-filtered backstepping, *International Journal of Control, Automation and Systems*, vol.22, no.5, pp.1601-1612, 2024.

[28] S. Gambhire, D. R. Kishore, P. Londhe and S. Pawar, Review of sliding mode based control techniques for control system applications, *International Journal of Dynamics and Control*, vol.9, no.1, pp.363-378, 2021.

[29] D. Liu and G.-H. Yang, Prescribed performance model-free adaptive integral sliding mode control for discrete-time nonlinear systems, *IEEE Transactions on Neural Networks and Learning Systems*, vol.30, no.7, pp.2222-2230, 2018.

Author Biography

Tinglong Pan received his B.Eng. degree in Industrial Automation from China University of Mining and Technology, Xuzhou, China, in 1999, and the Ph.D. degree in Power Electronics and Power Drive from China University of Mining and Technology, Xuzhou, China, in 2004.

He is currently a Professor at Jiangnan University, where his research interests include microgrid control technology, power conversion technology, power drive systemand its intelligent control technology.

Xiaobo Lu received his B.S. degree in Electrical Engineering and Automation from Nanjing Tech University, Nanjing, China, in 2022. He is currently pursuing the M.S. degree in Electrical Engineering with Jiangnan University, Wuxi, China.

His research interests include nonlinear system and its control technology.

Zhenlan Dou received the Ph.D. degree in Motors and Electrical Appliances from Shanghai Jiao Tong University, China, in 2013.

She has long been engaged in energy storage, micro grid, distributed energy, integrated energy system and its control technology research and engineering application demonstration. She is currently the Senior Expert of the State Grid Shanghai Municipal Electric Power Company.

Weilin Yang received his B.Eng. degree in Machine Design & Manufacture and Their Automation from University of Science and Technology of China, Hefei, China, in 2009, and the Ph.D. degree in Mechanical Engineering from City University of Hong Kong, Hong Kong SAR in 2013.

He was a postdoctoral researcher at Masdar Institute of Science and Technology (now Khalifa University), Abu Dhabi, UAE, 2013-2016. He was a research engineer of General Electric (GE) Global Research, Shanghai, 2016-2017. He joined Jiangnan University in July 2017, where he is currently an Associate Professor. His research interests include modeling and control of energy systems, robust model predictive control, and dada-driven control.

Dezhi Xu received the Ph.D. degree in Control Theory and Control Engineering from Nanjing University of Aeronautics and Astronautics, China, in 2013.

He was a Visiting Fellow with the Department of Biomedical Engineering, City University of Hong Kong, China, from 2018 to 2019. He is currently a Professor and Doctoral Supervisor with the Southeast University. His research interests include data-driven control, fault diagnosis and fault-tolerant control, multi-agent systems and cyber-physical systems, technologies of renewable energy, motor control, and smart grid. Dr. Xu was supported by the National Natural Science Fund for Excellent Young Scientists Fund Program in 2022. He was a recipient of the First Class Prize of Science and Technology Progression from the China General Chamber of Commerce in 2016, and the Best Young Scholar of Jiangnan University in 2022. He was a Guest Editor for the International Journal of Innovative Computing, Information and Control and the Electric Power. He currently serves as an Editorial Board Member for the International Journal of Innovative Computing, Information and Control, the Electric Power, the Electrotechnical Application and the Electrical Engineering. He is a Committee Member of the Association of Energy Internet, and Trusted Control in Chinese Association of Automation (CAA), and the Energy Storage in China Renewable Energy Society (CRES).